ISSN 1392-1320 MATERIALS SCIENCE (MEDŽIAGOTYRA). Vol. XX, No. X. 2027

In-situ EBSD Observation on Slip-less Fragmentation of Irregular-shaped Primary α Grains of Ti-6Al-4V-0.55Fe Alloy before Rupture

Zhangbin WU[1], Ketao WANG[1], Jiong ZHAO[2], Peng ZHANG[2], Zhenhua DAN[1*], Hui CHANG[1]

[1] *College of Materials Science and Engineering, Nanjing Tech University, Nanjing 210009, China*
[2] *Jiangsu Tiangong Technology Co., Ltd., Zhenjiang 212413, China*

http://doi.org/10.5755/j02.ms.44004

Received 4 January 2026; accepted 20 February 2026

In-situ SEM/EBSD characterization techniques were employed to investigate the microstructural evolution and characteristic deformation behavior of slip-lees fragmentation of irregular-shaped α grains in Ti-6Al-4V-0.55Fe alloy. The as-forged Ti-6Al-4V-0.55Fe alloy exhibits multiscale synergistic evolution during in-situ tensile deformation, including the changes in the fraction of the high-angle grain boundaries (HAGBs), the rotation of the grains, stress concentrations and dislocation slips. With increase of strains, cross slips and multi slips are activated after the single slips occur at the small strains. The HAGB proportion decreases while that of low-angle grain boundaries continues to increase. This transformation originates from strain-induced dislocation slip and rearrangement. The uniform plastic deformation of as-forged Ti-6Al-4V-0.55Fe alloy is mainly achieved by the activation of the pyramidal <c+a> slips. Within grains in high-strain regions, stress concentration causes a dramatic accumulation of orientation differences, inducing slip-less fracture of irregular-shaped primary α grains along specific internal paths at relatively low strain. In terms of crystallographic evolution, the grain rotation path activated by prismatic slip prefers (0001) basal plane, and promotes a synergistic effect of (0001) texture strengthening and (10-10) texture weakening. Structural inhomogeneities in the size and shape of primary α grains cause abnormal slip-less fragmentation during tensile deformation.
Keywords: Ti-6Al-4V-0.55Fe alloy, In-situ SEM/EBSD, slip-less fragmentation, activation of dislocation slip.

1. INTRODUCTION

Conventional Ti-6Al-4V alloy is widely utilized in the aerospace and marine industries due to its excellent mechanical properties/weight ratios and high corrosion resistance [1, 2]. Ti-6Al-4V alloy with a typically bimodal microstructure comprising of an equiaxed primary hcp-Ti (α_p) and a lamellar secondary hcp-Ti (α_s)/bcc-Ti (β). Among the three phases, dominant primary hcp-Ti (α_p) are able to resist plastic deformation in comparison to low proportional β phases [3, 4]. In fact, the active slip modes of the dominant α phase, accumulation of the back stress, the slip transmissions and activation of strain-induced dislocations are regarded as the main concerns during tension or compression [5 – 8]. From extant studies, the deformation mechanism of α_p in the bimodal Ti-6Al-4V alloy is still not completely understood. Moreover, different rotation paths and rotation rates resulted among the grains and within a single grain owing to the difference in active slip systems, and further influence the deformation behavior of α_p in Ti-6Al-4V alloys [9, 10].

Fe micro-alloying is considered as an effective route to promote the mechanical properties of Ti-6Al-4V alloy [11]. The optimized addition of 0.55 wt.% Fe has been reported previously from the aspects of tensile strengths and fracture toughness [12, 13]. Moreover, the addition of Fe helps to decrease the temperature of β transus and hot working, and the peak flow stress during hot rolling and forging [14]. As mentioned before, the geometry of α_p grains with relatively large size affects the accumulation of the back stress at the interfacial regions between phases and grains [7, 10]. Taking account of the grain size gradient, the large-sized grains and ultra-fine grains act as the "soft domains" and "hard domains" respectively during deformation. Grain size gradient, slip system compatibility, subgrain formation and multi-slip system activation play an important role in the generation of back stress. Due to the heterogeneous deformation behavior between large and small grains, dislocations accumulate at grain boundaries and induce back stress. Plastic deformation behaviors of Fe micro-alloyed Ti-6Al-4V alloys attract much attention due to the optimized mechanical performance and great potential for extended applications.

Here, some efforts have been made to investigate the different responses of slip lines, deformation of the grains, the accumulation of stress at the interfacial regions between grains and inside the grains, and the generation of dislocations inside by using in-situ anixial tensile testing method. The importance of the effects of the geometry of grains is explored through the comparison of geometrically necessary dislocations (GND), difference in Kernel average misoritentation (KAM), slip behavior of dislocations.

2. EXPERIMENTAL DETAILS

Ti-6Al-4V-0.55Fe bulks were purchased from Baoji Titanium Co. Ltd. The chemical composition of as-forged Ti-6Al-4V-0.55Fe alloy was 6.20 wt.% Al, 4.03 wt.% V, 0.537 wt.% Fe, 0.004 wt.% C, 0.043 wt.% O, 0.007 wt.% N and Ti balanced. Ti-6Al-4V-0.55Fe alloys were melted 3

* Corresponding author: Z.H. Dan
E-mail: *zhenhuadan@njtech.edu.cn*

times by the vacuum arc remelting (VAR) process. In the following forging process, the alloy was initially fabricated into as-cast Ti-6Al-4V-0.55Fe via three rounds of vacuum consumable arc melting. As-cast bars were then subjected to three forging processes with approximately 50 % at 1110 °C for 2 hours, approximately 50 % at 1010 °C for 1.5 hours, and approximately 85 % at 900 °C for 1.5 hours. The β transus temperature was determined to be 950 °C by combining the metallographic method and differential scanning calorimetry.

The specimens were prepared by wire electrical discharge machining (WEDM), and their dimensions are illustrated in the inset figures in Fig. 1a. In-situ tensile tests were carried out on an in-situ tensile stage equipped in a field emission scanning electron microscope (FESEM, TESCAN S8000 GMH) at a tensile rate of 2 μm s^{-1}. The observations by scanning electron microscopy (SEM) and electron backscatter diffraction (EBSD) were conducted under an accelerating voltage of 20 kV, working distance of 15 mm and step size of 0.6 μm.

3. EXPERIMENTAL RESULTS AND DISCUSSION

3.1. Activation of slips during in-situ tensile deformation characterized by in-situ SEM observation

Fig. 1 shows the displacement-load curve of the Ti-6Al-4V-0.55Fe alloy during in-situ tensile testing. The displacement-load curve is very typical and underwent several stages including the elastic stage, the yield stage, the work hardening stage and final rupture. The tensile elongation was paused at positions of 0 mm, 0.72 mm, 1.27 mm, 1.44 mm, and 1.77 mm marked as P_0, P_1, and P_2, respectively, in order to investigate the deformation from the captured SEM morphology. The as-forged Ti-6Al-4V-0.55Fe alloy in Fig. 1 b1 is composed of equiaxed α grains and some irregular-shaped α grains. The dominant phase is α phase, and β phase is in low proportion. When the displacement was 0.72 mm, there are several single slip lines in Fig. 1 b2 in the elastic stage. At the large displacement of 1.27 mm in the yield stage, many slip lines are generated and lined up, and the surface of the elongated sample becomes rougher accompanying with necking. Many cross-slip lines and multi-cross slip are activated as the displacement is 1.44 mm in the work hardening stage as shown in Fig. 1 b3. With the accumulation of the newly-formed dislocations inside the α grains and at the interfacial regions, the dislocations density inside the alloys is drastically increased due to large plastic deformation. As a result, the necking becomes more serious. It is worthy to state that the slip lines were hardly observed inside some specific grains. This fact indicates that the α grains with specific orientation may be insufficient to initiate deformation in the early stage of deformation. The accumulation of the dislocations and slip lines might link with the degree of plastic deformation.

3.2. Effect of the geometrical characteristic on the deformation of α_p grains on base of in-situ EBSD analysis

By tracking the changes of 6 specific α_p grains in the inverse pole, grain boundaries, Kernel average misoritentations, the density of geometrically necessary dislocations (GND) and the geometry at the same position during in-situ tensile testing, the plastic deformation had been investigated. These 6 grains were marked as A, B, C, D, E and F, and the different displacements were indicated by the "1, 2, 3", such as grain A3 for grain A at a displacement of 1.44 mm. Fig. 2 summarizes these changes based on the experimental results obtained from in-situ EBSD analysis. IPF maps at different displacements of 0 mm, 1.27 mm and 1.44 mm in Fig. 2 b1 – b3. Most of the α_p grains still maintain their initial oritentation without changes and serious rotations until the yielding stage. The geometry of α_p grains becomes slightly different. However, when the samples were subjected to the plastic deformation at the displacement of 1.44 mm, many subgrain boundaries form accompanying with the generation of small-sized subgrains as indicated in Fig. 2 b1 – b3.

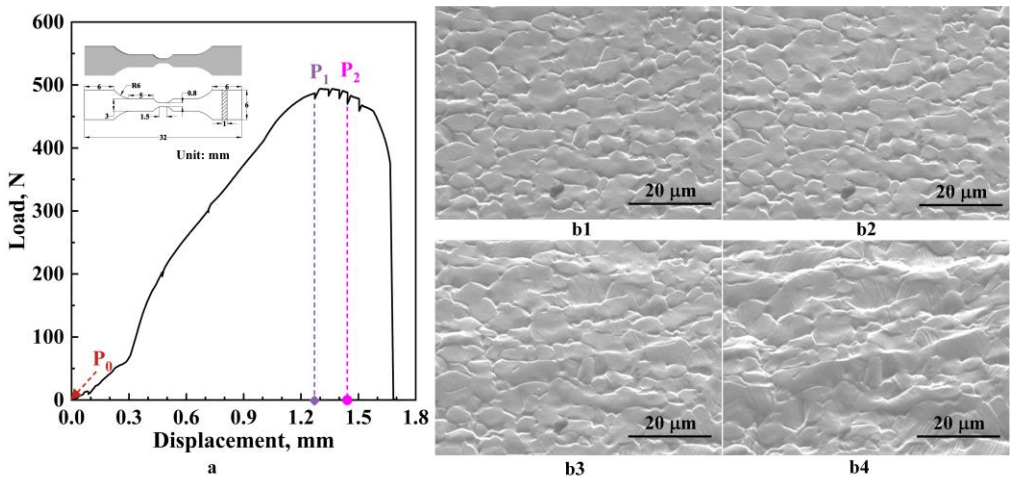

Fig. 1. a – In-situ load-displacement curve of Ti-6Al-4V-0.55Fe alloys during in-situ tensile test; b1 – the surface morphology at corresponding displacement of 0 mm; b2 – 0.72 mm; b3 – 1.27 mm; b4 – 1.44 mm. Tensile direction is horizontal. The inset shows the dimensions of the sample used for the in situ tensile tests

When no load is applied at P_0, the proportions of high-angle grain boundaries (HAGB marked as blue lines with misorientation higher than 15°) and low-angle grain boundaries (LAGB marked as red lines with misorientation lower than 15°) are 66.4 % and 33.6 %, respectively. When the displacement increases to 1.27 mm at P1, the LAGB fraction rises to 51.4 %, while HAGB fraction drops to 48.6 %.When the displacement further increases to 1.44 mm at P2, the LAGB fraction continue to increase up to 62.4 %, whereas that of LAGB inversely decreases down to 37.6 %. As result, the stress concentration becomes more serious at different strains as shown in Fig. 2 c1 – c3.

KAM value increases from 0.5° to 0.81° with an increase on the displacement of as-forged Ti-6Al-4V-0.55Fe alloy. The density of GND at a displacement of 1.27 mm is confirmed to be 6.4×10^{14} m^{-2} in Fig. 2 d. Under unloaded conditions, the strain is mainly distributed at the grain boundaries of the α phase. With the increase of plastic deformation, thestrain gradually extends from the grain boundaries to the interior of the α_p grains. As the tensile process proceeds, the GND density increases from 4.55×10^{14} m^{-2} to 8.91×10^{14} m^{-2}. The shapes of 6 grains are outlined in Fig. 2 e, and the deformation changes at different levels. The ratio of length-to-height is calculated to be 1.43 for grain A1, 1.61 for grain A2, 1.77 for grain A3, 2.76 for grain B1, 3.79 for grain B2, 4.86 for grain B3, 1.70 for grain C1, 2.13 for grain C2, 2.68 for grain C3, 0.94 for grain D1, 1.06 for grain D2, 1.29 for grain D3, 1.33 for grain E1, 1.09 for grain E2, 1.01 for grain E3, 1.51 for grain F1, 1.61 for grain F2, 1.96 for grain F3. As summarized in Fig. 2 f, GND density, texture intensity, KAM value and fraction of LAGB all increase with the displacements. Although the macroscopic plastic deformation takes place for all grains in Ti-6Al-4V-0.55Fe alloy, inhomogeneous deformation occurs inside due to structural inhomogeneities (such as grain size differences, and the geometry of grains, the rotation of grains, etc.), which then trigger subsequent mechanical responses.

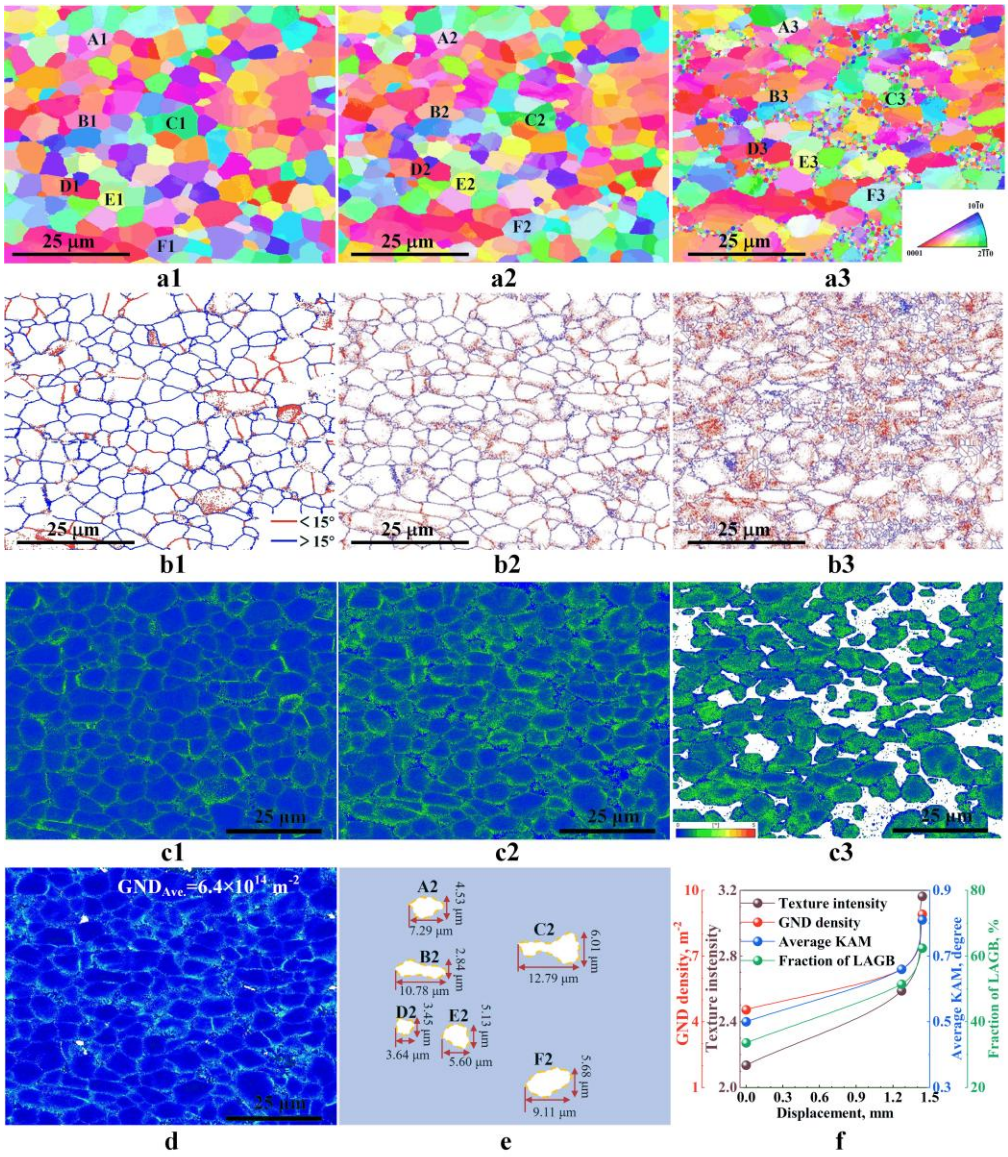

Fig. 2. a1, a2, a3 – corresponding inverse pole figures; b1, b2, b3 – distribution profiles of grain boundary, c1, c2, c3 – Kernel average misorientation mappings of Ti-6Al-4V-0.55Fe alloys at different displacement: a1, b1, c1 – 0 mm; a2, b2, c2 – 1.27 mm, a3, b3, c3 – 1.44 mm; d – the GND profile; e – the specific geometry outlines of grain A, B, C, D, E, F at a displacement of 1.27 mm and the dependency of GND density, texture intensity; f – average KAM and fraction of LAGB. Tensile direction is horizontal

The inhomogeneous deformation is linked with the density of dislocations, activation of the dislocation slips and the generation and strain distribution inside the grains and the interface regions between grains. Characteristic Schmid factor for slip systems of basal <a> for {0001}<11-20>, prismatic <a> for {1-100}<11-20> and pyramidal <c+a> for {1-101}<11-20>, often used to judge the difficulty to the activation of the dislocation slip, is displayed in Fig. 3 a1 – a3 . The pyramidal <c+a> has been activated as shown in Fig. 3 a3. As for grain A, B, D, E and F, more than two slip systems among the above-mentioned slip systems have been activated at the displacement of 1.27 mm. The KAM of grain A2 shows the higher strains at the edges of the grains due to the higher stress concentration in Fig. 3 b, although grain A2 has the ratio of length-to-height equal to 1.61. With the progress of stretching, the KAM values of grain A increase gradually. The increase in KAM values is attributed to the continuous accumulation of dislocations during the tensile process, which leads to a gradual increase in the misorientation between different regions inside the grains, thereby resulting in the gradual increase in KAM values. Grain A2 has the Schmid factor of 0.45 for the basal <a>, 0.21 for the prismatic <a>, and 0.38 for the pyramidal <c+a>. The large Schmid factor for basal <a> means that the basal slip systems are relatively easy to activate and basal slip is the main deformation mode of the grains during tensile elongation. The basal slip dominates in the initial stage and the pyramidal and prismatic slip systems are gradually activated at larger displacements to accommodate the deformation through gradual orientation adjustment and the grain rotations [15, 16]. The grain rotation of grain A and F is almost the same as 5°, and the rotation rates are confirmed to be 3.5 °/mm for grain A and 1.44 °/mm. The grain rotation for Grain B, C, D, E is 1 – 3°. The grain C has an irregular shape similar with dumb-bell, and the middle region is narrow. However, the ingrain strain inside grain C2 is very local with a displacement of 1.27 mm, particularly higher strain at the neck region in Fig. 3 c. The strain vertical to the tensile direction in the frame is obviously higher than in other interior regions. The misorientation angles along Line CD become larger at the displacement of 1.27 mm compared with those at the initial states, and the misorientation angle at the position with higher strain is even higher than 2°, which indicates the formation of the new subgrain boundaries there, as present in Fig. 3 d. The Schmid factors of all 6 grains C2 at a displacement of 1.27 mm (P1 position) are summarized in Fig. 3 e. The deformation in grain A is mainly achieved by the basal <a> slip, as well as for grain E. That of grain B is attributed to both basal <a> and pyramidal <c+a> slips, and that dominant operated slips as for grain D are both prismatic <a> and pyramidal <c+a> slips. It is worthy to state that grain F has a relatively low Schmid factor (0.31 for basal <a>, 0.06 for prismatic <a> and 0.19 for pyramidal <c+a> slips) which are resulted from the low degree of plastic deformation of the adjacent grains. However, the Schimd factors for grain C are confirmed to be 0.23 for basal <a>, 0.03 for prismatic <a> and 0.12 for pyramidal <c+a> slips. This fact means that almost all slip systems for grain C fail to be activated as other grains. It is considered that the slip-less plastic deformation occurrs at the relative low degree of strain.

Fig. 4 reveals the Schmid factor distribution maps of the deformed Ti-6Al-4V-0.55Fe alloys across different slip systems (basal <a>, prismatic <a>, and pyramidal <c+a> slip). As can be seen in Fig. 4 a, the Schmid factors of the pyramidal plane are mostly concentrated in the range of 0.4 – 0.5, with 63 % of them exceeding 0.4. In contrast, the Schmid factors of the prismatic <a> and basal <a> are mostly below 0.4 accounting for 38% and 25% for values greater than 0.4.

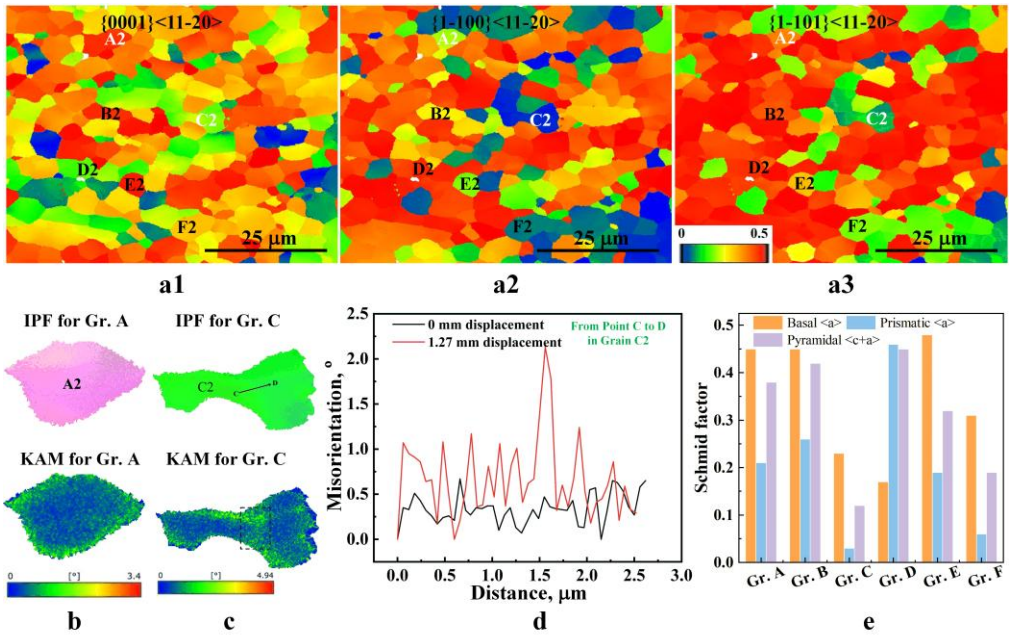

Fig. 3. Distribution maps of Schmid factors of Ti-6Al-4V-0.55Fe alloys at different displacement: a1 – 0 mm; b1 – 1.27 mm; c1 – 1.44 mm. The IPF and KAM for: b – grain A; c – grain C at displacement of 1.27 mm; d – comparison of misoritentation along line CD at displacement of 0 mm and 1.27 mm; e – the Schmid factors of grain A, B, C, D, E, F at displacement of 1.27 mm. Tensile direction is horizontal

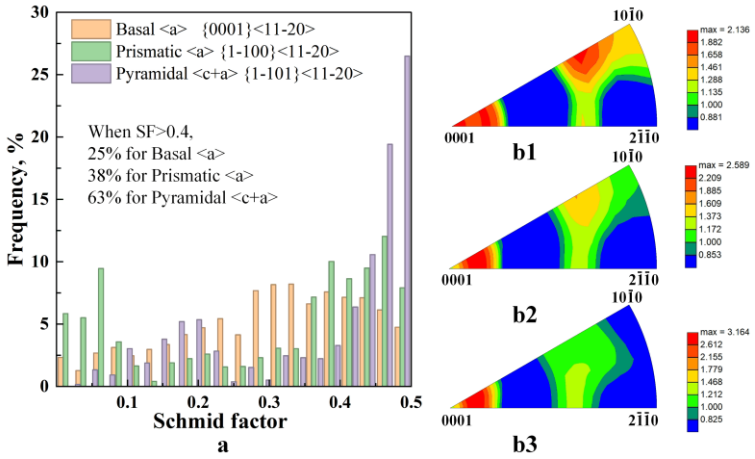

Fig. 4. a – distribution frequency and ratios of Schmid factors at displacement of 1.27 mm; b1 – IPF at different displacements of 0 mm; b2 – 1.27 mm; b3 – 1.44 mm of Ti-6Al-4V-0.55Fe alloys

Larger Schmid factor indicates that the corresponding slip system is more easily activated, which facilitates plastic deformation. It can thus be concluded that the deformation of the deformed Ti-6Al-4V-0.55Fe alloy is mainly induced by the pyramidal slip system, and this finding is consistent with the research results before [10, 13]. At the initial stage of tensile, due to the difficulty of slip, the grains may mainly coordinate the deformation with adjacent grains through grain rotation. The grain rotation path is related to the texture evolution of equiaxed α_p grains in titanium alloys [15]. It is evident that a similar phenomenon also occurs in the Ti-6Al-4V-0.55Fe alloy. The inverse pole figures (IPF) at different displacements during in-situ tensile testing in Fig. 4 b1 – b3 show that the texture intensity along the (10-10) direction gradually decreases with increasing displacement and strain. However, the texture intensity along the (0001) direction exhibits an opposite trend, increasing progressively as displacement and strain increase.

3.3 Discussion

As indicated in Fig. 2 a3, b3, c3, and Fig. 3 c, grain C has been fragmented under the interaction of the high stress at the necking region by the adjacent deformed grains. Among 6 grains tracked during tensile elongation, only grain C undergoes serious plastic deformation and fragmentation at a displacement of 1.44 mm. This fact is considered to depend on the geometrical characteris-tics of grain C and the lack of activation of the dislocation slip systems in the interior grain. As indicated by the Schimd factors of grain C presented in Fig. 3 e, the slip-less plastic deformation governs the stress redistribution inside grain C, and further results in the local formation of the subgrains at the necking regions in Fig. 3 c. During the in-situ tensile process, the degree of geometric shape change is relatively low for equiaxed grain A, D and E. The aspect ratio of grain A changed from 1.07 → 0.95 → 0.78, and that of grain D changed from 0.94 → 1.06 → 1.29, and that of grain E changed from 1.33 → 1.09 → 1.01. The uniform strain distribution at a low level is observed, and the serious plastic deformation does not take place for grain A, D and E. The abnormal fragmentation for grain C is considered to be due to the high local stress concentration and slip-less deformation. The irregular outlines of grain C trigger the uneven stress distribution and cause the higher strain at the necking region in Fig. 3 c. From the aspect of the dislocation slip, this kind of heterogeneity in the grain size and grain shapes for grain C prefers to drive the dislocations to accumulate at specific regions, such as the narrow regions between two adjacent tensile regions, the grain boundaries or the interface between two phases [7, 17]. Although the present Ti-6Al-4V-0.55Fe alloys are composed of α and β phases, the β grains are limited in proportion and small in size. The effect of the β grains is not taken into account for the plastic deformation here. Therefore, the abnormal fragmentation of grain C during plastic deformation is induced by the structural inhomogeneities of grain sizes and grain shapes. On the other hand, that means that the spheroidization and equiaxation of α_p grains during the forging, annealing and rolling is of importance for the improvement of the rupture resistance of titanium alloys.

4. CONCLUSIONS

In-situ SEM/EBSD technology was employed here to investigate the microstructural evolution and tensile fracture failure mechanism of Ti-6Al-4V-0.55Fe alloy. Macroscopically, as-forged Ti-6Al-4V-0.55Fe alloy exhibited a higher proportion of low-angle grain boundaries, larger local misoritentation, and more stronger stress concentration inside α_p grains during the in-situ tensile process. The uniform plastic deformation of as-forged Ti-6Al-4V-0.55Fe alloy is mainly achieved by the activation of the pyramidal <c+a> slips. During the deformation process, the grain rotation path activated by pyramidal slip gradually shifted toward the (0001) direction, which enhanced the intensity of the (0001) texture and weakened the intensity of the (10-10) texture. The structural inhomogeneities of large α_p grains with irregular shapes caused the abnormal fragmentation through the localization of the newly-formed dislocations. The rupture of the irregular-shaped α_p grains is attributed to their slip-less deformation.

Acknowledgments

This work is financially supported by the National Science and Technology Major Project of the Ministry of Science and Technology of China, the National Natural

Science Foundation of China (52371157&51671106), Frontier R&D Program Project of Jiangsu Province (BF2024008). This work is partially supported by Priority Academic Program Development of Jiangsu Higher Education Institution (PAPD).

REFERENCES

1. **Najafizadeh, M., Yazdi, S., Bozorg, M., Mouziraji, M.G., Hosseinzadeh, M., Zarrabian, M., Cavaliere, P.** Classification and Applications of Titanium and Its Alloys: A Review *Journal of Alloys and Compounds Communications* 3 2024: pp. 100019. https://doi.org/10.1016/j.jacomc.2024.100019
2. **Hémery, S., Villechaise, P.** On the Influence of Ageing on The Onset of Plastic Slip in Ti-6Al-4V at Room Temperature: Insight on Dwell Fatigue Behavior *Scripta Materialia* 130 2017: pp. 157 – 160. https://doi.org/10.1016/j.scriptamat.2016.03.018
3. **Wang,Q., Liu, Z.** Plastic Deformation Induced Nano-scale Twins in Ti-6Al-4V Machined Surface with High Speed Machining *Materials Science and Engineering A* 675 2016: pp. 271 – 279. https://doi.org/10.1016/j.msea.2016.08.076
4. **Liu, Y.G., Li, M.Q., Liu, H.J.** Deformation Induced Face-centered Cubic Titanium and Its Twinning Behavior in Ti-6Al-4V *Scripta Materialia* 119 2016: pp. 5 – 8. https://doi.org/10.1016/j.scriptamat.2016.03.018
5. **Zheng, Z., Waheed, S., Balint, D.S., Dunne, F.P.E.** Slip Transfer Across Phase Boundaries in Dual Phase Titanium Alloys and The Effect on Strain Rate Sensitivity *International Journal of Plasticity* 104 2018: pp. 23 – 38. https://doi.org/10.1016/j.ijplas.2018.01.011
6. **Zhang, S., Zeng, W., Zhao, Q., Ge, L., Zhang, M.** In Situ SEM Study of Tensile Deformation of a Near-β Titanium Alloy *Materials Science and Engineering A* 708 2017: pp. 574 – 581. https://doi.org/10.1016/j.msea.2017.10.028
7. **Meng, L.J., Wang, Y.Y., Li, X., Wang, Z.H., Jiang, Z.Y., Zhao J.W.** Origin of Back Stress Generation during Tensile Deformation of A Heterostructured Titanium Alloy: An In-situ EBSD Study on Local Slip System Activation *Journal of Materials Research and Technology* 38 2025: pp. 879 – 892. https://doi.org/10.1016/j.jmrt.2025.07.239
8. **Chun, Y.B., Battaini, M., Davies, C.H.J., Hwang, S.K.** Distribution Characteristics of Ingrain Misorientation Axes in Cold-rolled Commercially Pure Titanium and Their Correlation with Active Slip Modes *Metallurgical and Materials Transaction A* 41 2010: pp. 3473 – 3487. https://doi.org/10.1007/s11661-010-0410-4
9. **Chen, P., Mao, S.C., Liu, Y., Wang, F., Zhang, Y.F., Zhang, Z., Han, X.D.** In-situ EBSD Study of The Active Slip Systems and Lattice Rotation Behavior of Surface Grains in Aluminum Alloy during Tensile Deformation *Materials Science and Engineering A* 580 2013: pp. 114 – 124. https://doi.org/10.1016/j.msea.2013.05.046
10. **Saxena, A.K., Tewari, A., Pant, P.** Quantitative Analysis of Orientation and Near Neighbor Interaction Effects during Deformation of Polycrystalline Ti6Al4V *Materials Science and Engineering A* 648 2015: pp. 1 – 8. https://doi.org/10.1016/j.msea.2015.09.013
11. **Guo, Y.H., Niu, J.Z., Cao, J.X., Sun, Z.G., Dan, Z.H., Chang, H.** Relative Atrength of β Phase Stabilization by Transition Metals in Titanium Alloys: The Mo Equivalent from A First Principles Study *Materials Today Communications* 35 2023: pp. 106123. https://doi.org/10.1016/j.mtcomm.2023.106123
12. **Chen, F.W., Gu, Y.L., Xu, G.L., Cui, Y.W., Chang, H., Zhou, L.** Improved Fracture Toughness by Microalloying of Fe in Ti-6Al-4V *Materials and Design* 185 2020: pp. 108251. https://doi.org/10.1016/j.matdes.2019.108251
13. **Liao, Y., Bai, J.H., Chen, F.W., Xu, G.L., Cui, Y.W.** Microstructural Strengthening and Toughening Mechanisms in Fe-containing Ti-6Al-4V: A Comparison between Homogenization and Aging Treated States *Journal of Materials Science and Technology* 99 2022: pp. 114 – 126. http://doi.org/10.1016/j.jmst.2021.04.063
14. **Zhu, X.X., Chang, H., Xie, Y.J., Ding, L., Li, H., Cui, Y.W., Li, J.J., Tang, J., Zhou, L.** Hot Deformation Behavior of Two Kinds of TC4-xFe Alloys Based on Processing Map *Rare Metal Materials and Engineering* 46 2017: pp. 204 – 210. https://doi.org/10.1016/1002-185X(2017)S1-204-07
15. **Tan, C., Sun, Q., Xiao, L., Zhao, Y., Sun, J.** Slip Transmission Behavior across α/β Interface and Strength Prediction with A Modified Rule of Mixtures in TC21 Titanium Alloy *Journal of Alloys and Compounds* 724 2017: pp. 112 – 120. https://doi.org/10.1016/j.jallcom.2017.07.002
16. **Li, W.S., Yamasaki, S.G., Mitsuhara, M.T., Nakashima, H.H.** In Situ EBSD Study of Deformation Behavior of Primary α Phase in A Bimodal Ti-6Al-4V Alloy during Uniaxial Tensile Tests *Materials Characterization* 163 2020: pp. 110282 https://doi.org/10.1016/j.matchar.2020.110282
17. **Stapleton, A.M., Raghunathan, S.L., Bantounas, I., Stone, H.J., Lindley, T.C., Dye, D.** Evolution of Lattice Strain in Ti-6Al-4V during Tensile Loading at Room Temperature *Acta Materialia* 56 2008: pp. 6186 – 6196. https://doi.org/10.1016/j.actamat.2008.08.030

© Wu et al. *2027* Open Access This article is distributed under the terms of the Creative Commons Attribution 4.0 International License (http://creativecommons.org/licenses/by/4.0/), which permits unrestricted use, distribution, and reproduction in any medium, provided you give appropriate credit to the original author(s) and the source, provide a link to the Creative Commons license, and indicate if changes were made.